Polymer Journal (2016) 48, 253–258

www.nature.com/pj

ORIGINAL ARTICLE

X-ray study of molecular motions in the rotator phases of normal tricosane

Kazuo Kato

The molecular motions of normal tricosane in rotator phases were studied by X-ray diffraction. Three parameters indicating the degree of disorder due to the molecular motions were obtained by analyzing the diffuse scatterings on the first and second layer planes in the rotator-II phase. The average translation between nearest-neighboring molecules, Δ_t, was 0.2 Å. The average angle of deviation of the molecular plane from the direction connecting the molecular axes of two laterally neighboring molecules, Δ_φ, was found to be π/6 rad. A disorder parameter representing the extent of the fluctuation in the intermolecular distance, Δ_r, was estimated to be 0.6 Å. The obtained values show that the translational motion along and the rotational oscillation around the molecular axis are fairly restricted in the rotator phases.
Polymer Journal (2016) **48,** 253–258; doi:10.1038/pj.2015.115; published online 16 December 2015

INTRODUCTION

The rotator phases of normal paraffin are the intermediate phases between the low-temperature crystalline state and the melted state. Many nuclear magnetic resonance,[1,2] infrared and Raman,[3] calorimetric,[4] neutron scattering[5] and X-ray[6] studies on the rotator phases have been carried out since the work of Müller.[7] The concrete mechanism behind the molecular motions in the rotator phases is not known in detail, but studies using an approach based on X-ray diffraction have been carried out. For example, Strobl *et al.*[8] examined the disorder between lamellae by analyzing the 00l Bragg reflections of normal tritriacontane and described the molecular motion along the molecular axis. However, the relative motions between the nearest laterally neighboring molecules have barely been studied. Yamamoto *et al.*[9] researched the disorders caused by molecular motions in the rotator phases and the rotation around and the translation along the molecular axes using mixtures of normal C_{17} and C_{18} alcohols as samples. There is a difference in chemical structure between normal paraffin and alcohols. We do not know how the difference in chemical structure influences the molecular motions. Hence we used tricosane, a normal paraffin of carbon number 23, as sample. We examined the diffuse scatterings that appeared on the first and second layer planes of the subcell. In our previous work,[10] these diffuse scatterings were analyzed quantitatively, and an orientational order in the rotator phases was found. Specifically, the molecular planes of two, or even three, laterally neighboring molecules were found to be oriented in the same direction, linking their molecular axes so that the molecules formed a row. In addition, we showed that ~60% of the molecules belonged to any one of the rows of molecules.

Thermal motion in the rotator phase causes a disorder in the molecular positions along the molecular axis as well as a disorder in the orientation of the molecular planes. It also causes disorders in the distance between adjacent molecules. In this paper, three disorder parameters related to the thermal motion of the molecules composing a row were found upon analyzing the experimental data obtained in our previous study.[10] Moreover, the thermal motions in the rotator phases will be discussed based on these parameters.

EXPERIMENTAL PROCEDURE

The samples consisted of normal tricosane $C_{23}H_{48}$ (Eastman Kodak Co., Rochester, New York, NY, USA), which contained a small amount of impurities (<5%). To prepare single crystals, the samples were dissolved in toluene, and thick single crystals were obtained by slow evaporation from a solution maintained at a temperature of 279 K. A flat-plate camera, a Weisenberg camera and a Bouman camera were used to visualize the diffuse scatterings. A schematic drawing of the Bouman camera is shown in Figure 1 (reprinted from ref. 10). This camera has a circular film that is positioned perpendicular to the rotation axis of the sample being analyzed. Furthermore, the camera was devised so that the rotation of the film would correspond to that of the sample. Figure 1 shows the setup of the camera, in which the crystal being analyzed is inclined in the direction of the incident beam. Thus, the diffraction pattern of the first layer plane is projected on the film.

The X-rays (MoK_α or CuK_α) were made monochromatic with a single crystal of graphite. The wavelengths of MoK_α and CuK_α are 0.7107 and 1.5418 Å, respectively. The intensity of the films was measured by a microphotometer (Nalumi Co., Ltd, Japan).

During the X-ray measurement, a sample was heated in a copper cylinder wrapped by nichrome wire. The temperature of the samples was controlled within ±0.1 K by a Cr–Ar thermocouple.

RESULTS AND DISCUSSION

To discuss the molecular motions in the rotator phases, the molecular structure will be treated as follows. The molecules have a rigid planer

Shizuoka Kita Senior High School, Shizuoka, Japan
Correspondence: K Kato, Shizuoka Kita Senior High School, 5-14-1, Sena, Aoiku, Shizuoka 420-0911, Japan.
E-mail: katok@shizuokakita-h.ed.jp
Received 15 July 2015; revised 23 October 2015; accepted 27 October 2015; published online 16 December 2015

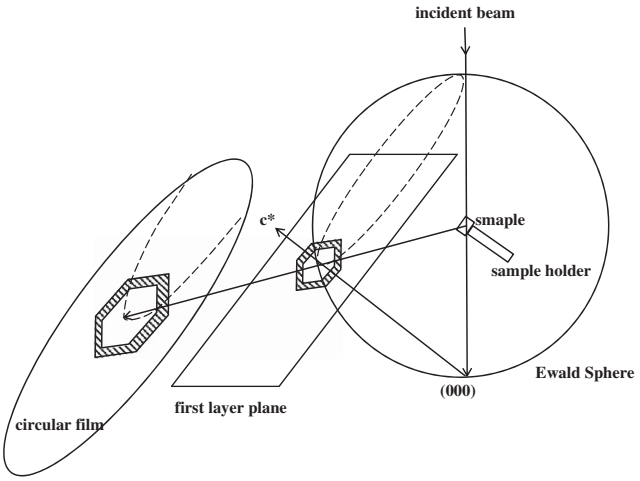

Figure 1 Schematic drawing of a Bouman camera (from ref. 10).

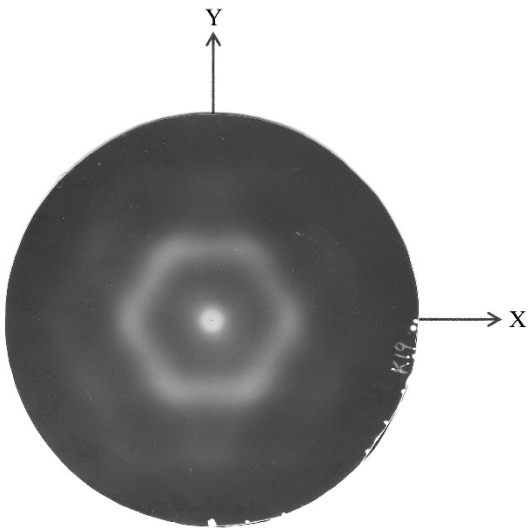

Figure 2 Diffraction pattern of the first layer plane of the subcell obtained by the Bouman method at 319 K. Monochromatic CuK$_\alpha$ rays were used (from ref. 10).

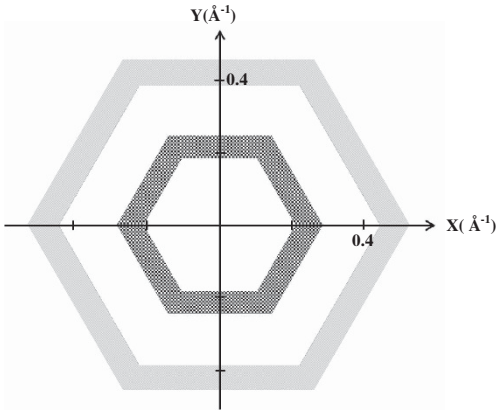

Figure 3 Simplified schematic drawing of Figure 2, where the coordinates of the reciprocal space of the first layer plane are used. Part of the shadow shows the region where the X-ray diffuse scattering on the first layer plane is mainly distributed.

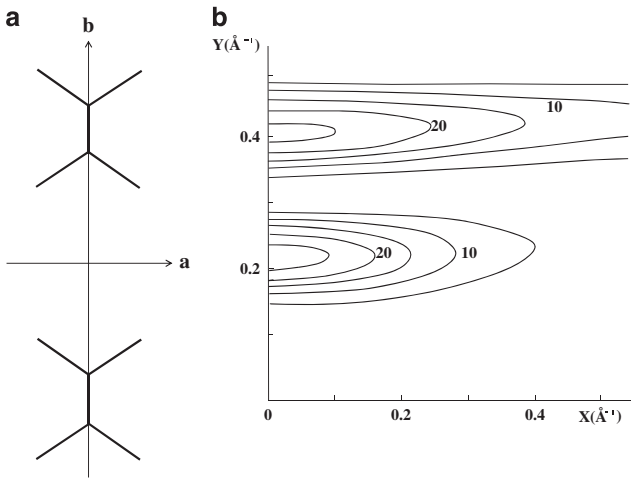

Figure 4 (**a**) Model of a row consisting of two molecules. (**b**) The diffraction pattern of the two-molecule row.

zigzag conformation, and all the intra-chain defects such as kinks are ignored.

Strobl *et al.*[8] reported that there were intra-chain defects that reduced the effective length of a chain in the rotator phases of *n*-tritriacontane. In our measurement on tricosane, however, such a result—the reduction of the effective chain length—was not notably observed. The chain length of a tricosane molecule is relatively short. Even if intra-chain defects exist, its percentage per molecule is small. The results obtained below will not be affected by adopting the above-described model.

Distribution of the number of molecules forming a row

Tricosane has three stable rotator phases during the heating process: the R_V ($313\,K \leqslant T < 315\,K$), R_I ($315\,K \leqslant T < 318\,K$) and R_{II} ($318\,K \leqslant T < 320\,K$) phases.[11,12] The R_V phase has a monoclinic form. In our previous measurement,[10] its molecular axis was tilted by 7.5° from the surface normal of the lamella toward the a axis, where the a axis corresponds to that of the low-temperature orthorhombic subcell. In addition, the subcell of the R_V phase is orthorhombic. The R_I phase has an orthorhombic form, and the molecular axis becomes parallel to the surface normal of the lamella. Its subcell is also orthorhombic. Both the R_V and the R_I phases have two layers in their unit cell. The R_{II} phase has a trigonal form consisting of three layers in the unit cell. Its subcell is hexagonal (see ref. 12 for details).

Figure 2 shows the diffraction pattern of the first layer plane of the R_{II} phase at 319 K, which was obtained with a Bouman camera in our previous work.[10] A schematic representation of Figure 2 is shown in Figure 3, where the coordinates of the reciprocal space on the first layer plane, X–Y, are introduced. This pattern has three-fold symmetry. However, the total pattern can be regarded as a superposition of three types of equivalent patterns. Figure 4b shows one of these X-ray patterns, which was obtained for the row of molecules shown in Figure 4a. To calculate the intensity distribution in Figure 4b, the molecular scattering amplitude of a tricosane molecule in the all-trans conformation was used. In the row shown in Figure 4a, the molecular planes are all oriented along the b axis of the original low-temperature orthorhombic form. Moreover, the molecules forming the row have an almost equal CH_2 level. Otherwise, the elongated pattern in Figure 2 cannot be formed. We denoted this X-ray pattern as I_{b^*}. The other two patterns can be obtained by rotating I_{b^*} by $\pm 60°$

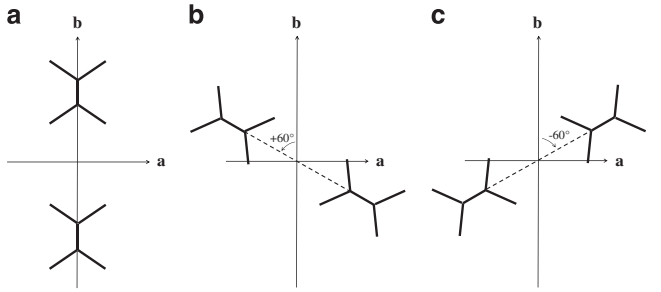

Figure 5 Three types of rows consisting of two molecules: (**a**) the row oriented along the b axis; (**b**) the row rotated by +60°; and (**c**) the row rotated by −60° around the c axis.

around the Z axis in the reciprocal space and denoted $I_{\pm 60}$. From these analyses,[10] it was found that three types of rows of molecules exist, whose directions are oriented along the b axis and rotated by $\pm 60°$ around the c axis (see Figure 5). In the R_{II} phase, the three types of patterns were identical. As a result, only the I_{b^*} pattern was analyzed.

The half width of the profile near $Y = 0.21\ \text{Å}^{-1}$ along the Y axis in Figure 2 can be used to roughly estimate the average number of molecules composing the rows. To obtain more accurate results, we analyzed the intensity along the Y axis of the first layer plane using a Fourier transform. In our previous work,[10] $g(M)/M$ was introduced as the ratio of the number of rows with M molecules to the total number of rows. And $g(M)$ itself represents the total number of molecules composing rows of M molecules. For example, $g(1)$ expresses the total number of molecules that are not in a row, while $g(2)$ or $g(3)$ corresponds to the total number of molecules composing rows of two or three molecules, respectively, and so on.

The intensities given by the rows of molecules are assumed to be incoherent with each other. Thus, the diffraction intensity I_{b^*} is given by the summation over all M of the product of $g(M)/M$ and the Laue function, $\sin^2\pi MbY/\sin^2\pi bY$,

$$I_{b*} = \sum_M \frac{g(M)}{M} \frac{\sin^2 \pi MbY}{\sin^2 \pi bY}, \tag{1}$$

where b is the average distance (4.75 Å) between nearest-neighboring molecules at 319 K. Let $V(y)$ denote the inverse Fourier transform of Equation (1):

$$V(y) = \int_{-\infty}^{+\infty} I_{b*} \exp(-2\pi iyY) \mathrm{d}Y. \tag{2}$$

The inverse Fourier transform of the Laue function gives the self-convolution of the disposition function $\Sigma_j \delta(y - jb)$:

$$\int_{-\infty}^{+\infty} \frac{\sin^2 \pi MbY}{\sin^2 \pi bY} \mathrm{e}^{-2\pi iyY} \mathrm{d}Y = \sum_{m=0}^{M-1} (M - m)\delta(y \pm mb), \tag{3}$$

where $\delta(y)$ is a delta function. Substituting Equations (1) and (3) into Equation (2) and rearranging Equation (2) yield the following equation:

$$g(M)/M = V((M-1)b) + V((M+1)b) - 2V(Mb). \tag{4}$$

In the transform of Equation (2), the data in Figure 6 (reprinted from ref. 10) representing the intensity distribution along the Y axis on the first layer plane were used after the necessary corrections, such as the background, Compton scattering and polarization, were applied. Moreover, the data were divided by the square of the molecular scattering amplitude of a tricosane molecule. Then, the integral in

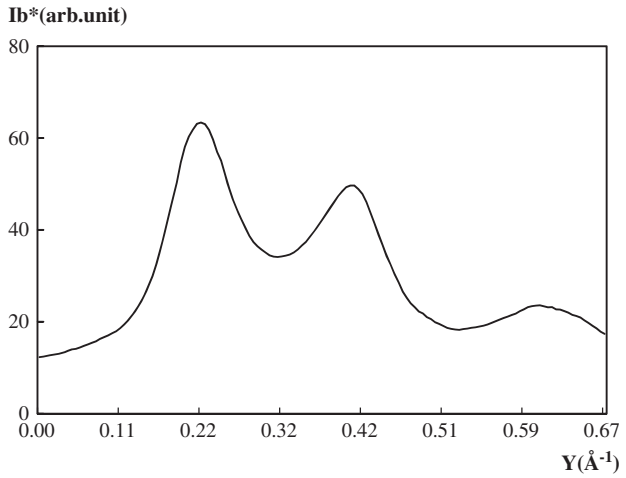

Figure 6 The intensity distribution for the first layer plane; the intensity was scanned along the Y axis in the reciprocal space. The solid line indicates the intensity along the Y axis in the R_{II} phase at 319 K. Monochromatic MoK$_\alpha$ rays were used (from ref. 10).

Equation (2) was calculated within the $1/(2b) \leqslant Y \leqslant 3/(2b)$ range because I_{b^*} becomes a periodic function of Y. The above Fourier transform is an application of the method developed by Bertaut.[13] The set of values for $g(M)$ in the R_{II} phase was obtained in our previous work.[10] The results are expressed in percentages, as follows:

$$g(1) = 42\%, g(2) = 42\%, g(3) = 13\% \text{ and } g(4) = 3\%. \tag{5}$$

The above results for the R_{II} phase show that 58% of the molecules in the crystal belong to any one of the rows of molecules and that 72% of the molecules belonging to rows of molecules consist of the row of two molecules.

Disorder by translational motion along the molecular axis

The diffraction patterns for the (002) and (004) reflections of the orthorhombic subcell become diffuse in the rotator phases. The intensity distribution along the meridian is shown in Figure 7a (reprinted from ref. 10). The square of the scattering amplitude of a CH_2 unit, $f_{CH_2}{}^2$, can be approximately replaced by $f_C{}^2 + 2f_H{}^2$, where f_C is the atomic scattering factor of a carbon atom and f_H is that of a hydrogen atom. The Fourier integral of the intensity distribution along the meridian

$$\int \left\{ I/\left(N f_{CH_2}{}^2\right) - 1 \right\} \cos(2\pi zZ) \mathrm{d}Z \tag{6}$$

produces a distribution function $L(z)$, which indicates the distribution obtained by projecting the CH_2 units onto the z axis. Here N denotes the number of CH_2 units. The result for the R_{II} phase is shown in Figure 7b (reprinted from ref. 10). The molecules composing a row had an almost equal CH_2 level, as mentioned in section 'Distribution of the number of molecules forming a row'. The translational disorder parameter Δ_t is defined as the average translation along the z axis between the nearest-neighboring molecules in a row. When the crystal has the low-temperature orthorhombic form, $L(z)$ will have sharp peaks around $z = 1.27$ Å, 2.54 Å and so on. In the rotator phases, the translational disorder makes the peaks of $L(z)$ curve broad as shown in Figure 7b. The value of Δ_t was estimated from the half-value width of the peaks in the curve presented in Figure 7b:

$$\Delta_t = 0.2\ \text{Å}. \tag{7}$$

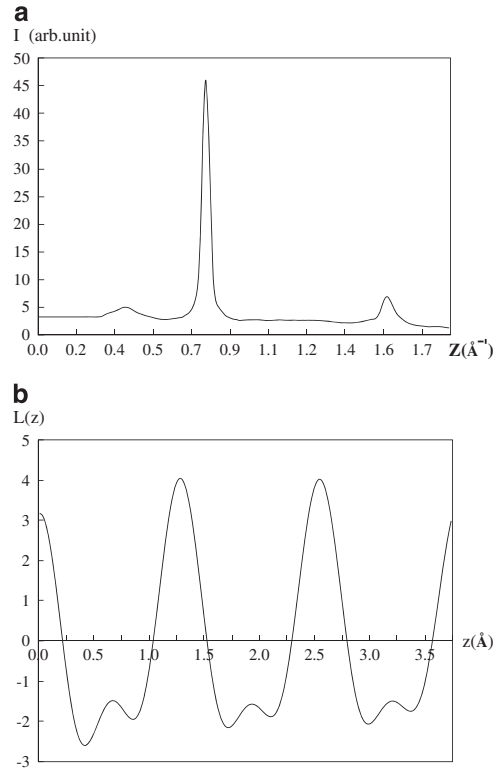

Figure 7 (**a**) Intensity distribution along the meridian obtained from the Weisenberg photograph at 319 K. Monochromatic MoK_α rays were used (from ref. 10). (**b**) Distribution function projecting the CH_2 units onto the z axis (from ref. 10).

This value is ~8% of the repeat distance of 2.54 Å and is quite small. The data in Figure 7a were obtained up to the 004 lattice point of the subcell. If the data were extended to the 006 lattice point, the peak of the distribution function in Figure 7b would become sharper and Δ_t would become smaller than 0.2 Å.

The oscillation frequencies of X-rays are high compared with the vibrational frequencies of molecules. Thus, the distribution functions obtained by X-ray diffraction indicate not only space average values but also time average values. The above results therefore show that each molecule in the row undergoes a very small amount of translational motion.

Disorder by rotational oscillation around the molecular axis in the R_{II} phase

The molecular planes of the molecules composing a row are not necessarily strictly oriented in the direction of the row. Rather, owing to rotational oscillation, the orientations of the molecular planes continually deviate from the direction of the row. A distribution of the frozen conformations of the molecular planes at each instant will be examined below.

Notably, $g(2)$ has the maximum value in the $g(M)$ set, with the exception of $g(1)$ (Equation (5)). On the basis of Equation (5) and comparing the intensity of the peak at $Y = 0.21\ \text{Å}^{-1}$ for the row of M molecules given in Figure 6, it was found that the diffraction by the rows of two molecules has an intensity 2.2 times greater than that by the rows of three molecules and 7.0 times greater compared with the rows of four molecules. As a result, the calculations were carried out assuming that the rows were all composed of two molecules. The diffraction pattern on the first layer plane was calculated using two

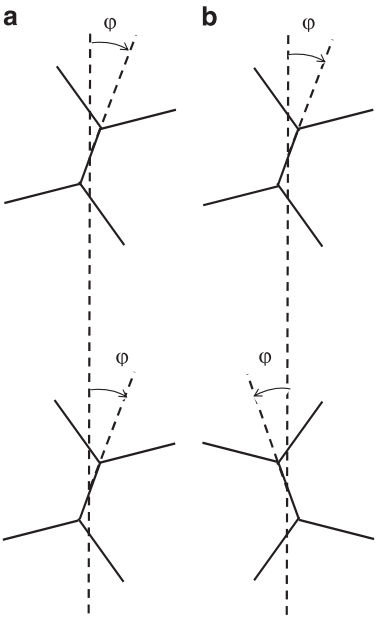

Figure 8 Two models of the pair of molecules: (**a**) the molecular plane of each molecule deviates by the same angle φ and (**b**) one molecule deviates by $+\varphi$ and the other by $-\varphi$.

models (a) and (b) as shown in Figure 8, where φ is the angle of deflection from the direction of the row. In model (a), the molecular plane of each molecule deviates by the same angle φ from the direction connecting their molecular axes. In model (b), one molecule deviates by $+\varphi$ and the other by $-\varphi$. Because the two molecules are oscillating independently around their molecular axes, φ is different for each molecule. However, any pair of φ can be roughly classified in model (a) or (b). To estimate the disorder by rotational oscillation, the X-ray patterns based on model (a) and (b) were calculated for various φ: φ was varied at intervals of $\pi/24$ from 0 to $\pi/4$. The calculated X-ray patterns were compared with Figures 2 and 3. We denote Δ_φ as the limit of φ at which the discrepancy between the observed and the calculated patterns arises: Δ_φ represents the average deviation of the molecular plane from the direction of the row. The results for $\varphi = 0$ and for $\varphi = \pi/8$ in model (a) are shown in Figures 4b and 9, respectively. In Figure 9, the position of the first peak on the Y axis gradually shifts along the direction parallel to the X axis with increasing φ. When φ reaches $\pi/8$, the first peak lies in a direction that is rotated around Z axis by approximately $\pi/5$ from the Y axis. On the other hand, the peak must lie within the direction that was rotated by $\pi/6$ from the Y axis, judging from Figures 2 and 3. Thus, a value of $\pi/8$ was adopted as Δ_φ in model (a).

The result for $\varphi = \pi/6$ in model (b) is shown in Figure 10, where a new diffuse scattering appeared with a peak position at ($0.3\ \text{Å}^{-1}$, $0.1\ \text{Å}^{-1}$) in the reciprocal space and was elongated in the direction parallel to the X axis. The intensity of this diffuse scattering became stronger with increasing φ. Such a diffuse scattering, however, was never observed before. Based on this result, $\pi/6$ rad was adopted as Δ_φ for model (b). The difference in Δ_φ between models (a) and (b) is small. Thus, we adopted $\pi/6$ rad, which is a larger value, as the value of Δ_φ:

$$\Delta_\varphi = \pi/6 \text{ rad.} \tag{8}$$

Considering the previous discussion on space averaging and time averaging for this case, the obtained value indicates that the degree of rotational oscillation is smaller than expected.

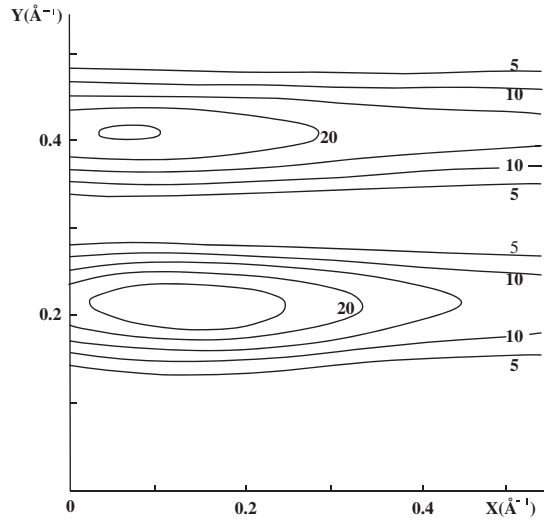

Figure 9 Calculated intensity distribution for $\varphi = \pi/8$ rad for model (a) in Figure 8.

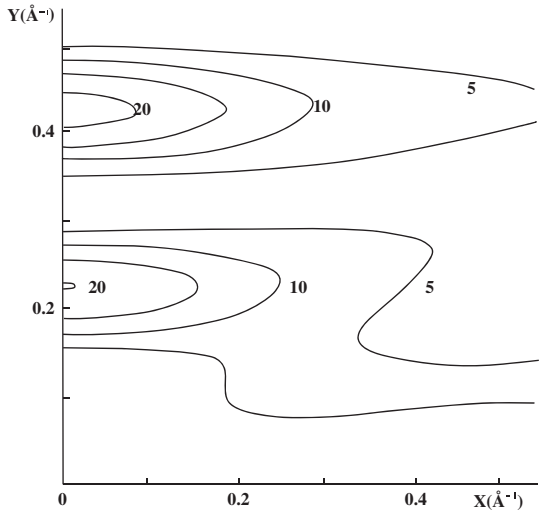

Figure 10 Calculated intensity distribution for $\varphi = \pi/6$ rad for model (b) in Figure 8.

Fluctuation in the distance between adjacent molecules

Thermal motion in the rotator phases causes fluctuations in the distance between the adjacent molecules forming a row. These fluctuations lower the ratio of the intensity of the second peak relative to the first peak on the first layer plane (Figure 6). On the other hand, the disorder resulting from the rotational and translational motions of the molecules hardly influences the value of this ratio. We estimated the fluctuations by comparing the model with the observed intensity. The model was limited to a row of two molecules as mentioned in section 'Disorder by rotational oscillation around the molecular axis in the R_{II} phase'. Furthermore, we assumed that the distance between the molecules forming a row followed a Gaussian distribution, mainly centered at 4.75 Å, which is the average distance between the nearest-neighboring molecules in the R_{II} phase. Thus, the distribution function was expressed as

$$\exp\left(-(r-4.75)^2/2\Delta_r^2\right)/\left(2\pi\Delta_r^2\right)^{1/2}, \tag{9}$$

where r is the distance between two molecules and Δ_r is the width of the fluctuation in the intermolecular distance. The intensity distributions were calculated for various values of Δ_r. The intensity distributions for $\Delta_r = 0$ and 0.60 Å are shown in Figure 11, and the observed intensity for the R_{II} phase is added to the figure. Adopting this approximation, in which the intensity of $g(M)$ is ignored for all values except $g(2)$, the intensity ratio of the second peak to the first peak of the profile calculated using $\Delta_r = 0.60$ Å gives the best agreement with that of the observed profile. We therefore adopted

$$\Delta_r = 0.60 \text{ Å}. \tag{10}$$

The root mean square displacement that is usually used, $\Delta_r' = \Delta_r/\sqrt{2}$, is 0.42 Å. This value is ~9% of the distance between the nearest-neighboring molecules and is somewhat large.

Concluding remarks

The results described above provide several insights regarding molecular motions in the rotator phases. Approximately 60% of all the molecules in the R_{II} phase undergo rotational oscillation while keeping the average direction of their molecular planes oriented in the direction of the row. The parameter corresponding to the disorder by rotation, $\Delta_\varphi = \pi/6$ rad, gives the degree of rotational oscillation.

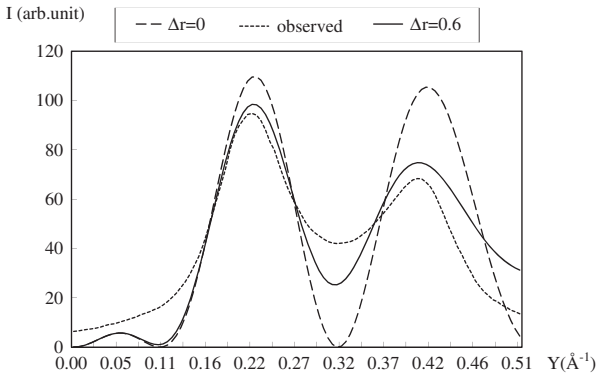

Figure 11 Intensity distributions for various values of Δ_r. The broken line indicates the intensity for $\Delta_r = 0$ Å, the solid line is for $\Delta_r = 0.6$ Å and the dotted line indicates the observed intensity in Figure 6.

The parameter for disorder by translation, $\Delta_t = 0.2$ Å, is small. The molecular motions in the row are fairly restricted, judging from the values of Δ_φ and Δ_t. Namely, the short-range order in the row is kept very high. On the other hand, the molecules abruptly lose their short-range order in the domain outside of the row of molecules.

The rotational jump model[2,14] stating that molecules undergo drastic rotations around their molecular axes that lead to the different directions of their molecular planes is influential. Because the mechanism of rotational motion in the rotator phases is based on this model, it can be explained as follows: the molecule belonging to a row rotationally oscillates around the direction of the row, although the motion is fairly restricted. Then, the molecule suddenly undergoes a drastic rotation around its molecular axis by either +60° or −60°. This molecule then influences the nearest-neighboring molecules to orient their molecular planes in the same plane that contains their molecular axes. As a result, the molecule causes its neighboring molecules to experience drastic rotations. The drastic rotations will generate a new row of molecules. If the conditions are favorable in a row of two molecules, it can grow into a row consisting of three molecules.

The above mechanism provides information about the crystallization process from the isotropic melt toward the low-temperature crystalline phase. When the crystallization begins, the hexagonal

subcell is formed first. The ordering of the molecular planes of neighboring molecules occurs: the molecules are oriented in the same direction that connects their molecular axes. The total number of molecules belonging to each of the three directions of the rows (Figure 5) is equal (refer section 'Distribution of the number of molecules forming a row'). By further cooling, the R_I phase appears, and the directions of the a–b axes of the orthorhombic subcell are determined. The order of the molecular planes in the R_I phase increases more than that in the R_{II} phase. Precise analysis using the data from our previous work[10] showed that the rows oriented along the b axis had 1.5 times more molecules than the rows oriented along the directions that were rotated by +60° or − 60°. From this result, we can deduce that the probability of the drastic rotation from the b axis to the direction rotated by +60° or − 60° is smaller than the probability of the drastic rotation in the reverse direction. Namely, the molecules in the R_I phase tend to orient their molecular planes toward the b axis rather than the other two directions.

The driving force that causes the molecular planes of the nearest-neighboring molecules to orient in the direction connecting their molecular axes remains unclear. Elucidating this mechanism is an important challenge for future research.

CONFLICT OF INTEREST

The author declares no conflict of interest.

1 Andrew, E. R. Molecular motion in certain solid hydrocarbons. *J. Chem. Phys.* **18**, 607–618 (1950).
2 Ewen, B., Fischer, E. W., Piesczek, W. & Strobl, G. Defect structure and molecular motion in the four modifications of n-tritriacontane. II. Study of molecular motion using infrared spectroscopy and wide-line nuclear magnetic resonance measurements. *J. Chem. Phys.* **61**, 5265–5272 (1974).
3 Unger, G. & Masic, N. Order in the rotator phase of n-alkanes. *J. Phys. Chem.* **89**, 1036–1042 (1985).
4 Sirota, E. B. & Singer, D. M. Phase transition among the rotator phases of normal alkanes. *J. Chem. Phys.* **101**, 10873–10882 (1994).
5 Doucet, J. & Dianoux, A. J. Rotational diffusion in the rotator phase of n-alkanes. *J. Chem. Phys.* **81**, 5043–5045 (1984).
6 Piesczek, W., Strobl, G. R. & Malzah, K. Packing of paraffin chains in the four stable modifications of n-tritriacontaine. *Acta Crystallogr.* **B30**, 1278–1288 (1970).
7 Müller, A. An X-ray investigation of normal paraffins near their melting points. *Proc. R. Soc. London Ser. A* **138**, 514–530 (1932).
8 Strobl, G., Ewen, B., Fisher, E. W. & Piesczek, W. Defect structure and molecular motion in the four modifications of n-tritriacontane. I. Study of defect structure in the lamellar interfaces using small angle x-ray scattering. *J. Chem. Phys.* **61**, 5257–5264 (1974).
9 Yamamoto, T., Nozaki, K. & Hara, T. X-ray and thermal studies on the rotator phases of normal higher alcohols $C_{17}H_{35}OH$, $C_{18}H_{37}OH$, and their mixtures. *J. Chem. Phys.* **92**, 631–641 (1990).
10 Kato, K. & Seto, T. Orientational order of normal paraffin chains in the rotator phases of tricosane. *Jpn J. Appl. Phys.* **41**, 2139–2145 (2002).
11 Seto, T. & Kato, K. Order of molecular packing in rotational phase of normal paraffin. *Polym. Prepr. Jpn* **28**, 421 (1979) [in Japanese].
12 Sirota, E. B., King, H. E., Singer, D. M. & Shao, H. H. Rotator phases of the normal alkanes: an x-ray scattering study. *J. Chem. Phys.* **98**, 5809–5824 (1993).
13 Bertaut, E. F. Raies de Debye-Scherrer et repartition des dimensions des domaines de Bragg dans les poudres polycristallines. *Acta Crystallogr.* **3**, 14–18 (1950).
14 Yamamoto, T. Monte Carlo simulation of the crystal structure of the rotator phase of n-paraffins. II. Effects of rotation and translation of the rigid molecules. *J. Chem. Phys.* **89**, 2356–2365 (1988).